

Optical Soliton Propagation in a Free-Standing Nonlinear Graphene Monolayer with Defects

Frederick Ira Moxley III,¹ Tim Byrnes,² Adarsh Radadia,³ and Weizhong Dai⁴

*¹Hearne Institute for Theoretical Physics,
Department of Physics & Astronomy,*

Louisiana State University, Baton Rouge, LA 70803, USA

*²National Institute of Informatics, 2-1-2 Hitotsubashi,
Chiyoda-ku, Tokyo 101-8430, Japan*

³Institute for Micromanufacturing, Louisiana Tech University, Ruston, LA 71272, USA

*⁴Mathematics & Statistics, College of Engineering & Science,
Louisiana Tech University, Ruston, LA 71272, USA*

Abstract

Recently, optical soliton propagation in an intrinsic nonlinear graphene monolayer configuration has been discovered. However, optical soliton behavior in a free-standing graphene monolayer with defects has not yet been studied. The objective of this article is to employ the generalized finite-difference time-domain (G-FDTD) method to efficiently simulate bright optical solitons, illustrating propagation of the electric field distribution in a free-standing nonlinear layer with variation in nonlinearity along its width. These variations of nonlinearity along the width represent graphene impurities, or defects. Results show that solitons propagate effectively even in the presence of strong spatial variations in the nonlinearity, implying the robustness of the medium with respect to optical propagation.

I. INTRODUCTION

Recently, the isolation of graphene monolayers from bulk graphite has inspired many studies [1], including those related to optical and opto-electronical applications [2, 3]. Findings show that photon propagation can be better controlled in materials with increasing nonlinear optical susceptibility [4, 5], which allows formation of temporal and spatial electro-magnetic (EM) solitons [6, 7]. Such structures are of high interest in optical communications. In the optical regime, Nesterov and co-workers [8] have used finite element modeling (FEM) to demonstrate that 2D graphene monolayers can support such a quantum phenomenon in the absence of defects. However, more realistically the graphene will have inhomogeneties in various parameters such as the interaction. Such parameter deviation can cause optical scattering, leading to loss of the optical soliton for large propagation distances. It is our understanding that such deviation in the parameters is rather difficult to simulate using finite element methods as they induce numerical instabilities, particularly for strong spatial variations. The motivation of this study is to employ our recently developed generalized finite-difference time-domain (G-FDTD) method [9] to solve a non-homogenous vector Helmholtz equation analogue. The G-FDTD scheme was developed for solving linear and nonlinear Schrödinger equations [9, 10]. It is explicit, permits an accurate solution with simple computation, and also satisfies a discrete analogue of the mass conservation law for nonlinear Schrödinger equations. In this study, we will use the G-FDTD method to simulate graphene imperfections in a free-standing configuration, permitting an analysis of the robustness of the optical soliton propagation. We will investigate whether or not these optical solitons propagate with great stability in the presence of very large spatial inhomogeneties. This will illustrate the effectiveness of the monolayer configuration for optical soliton propagation and allow us to examine the robustness of the soliton propagation under non-ideal conditions.

II. HELMHOLTZ'S EQUATION APPROXIMATION

In this study, we consider a single graphene monolayer placed inside a planar linear dielectric waveguide, as shown in Figure 1. The vertical confinement along the y -axis provides a direction for the propagating EM mode. We assume that graphene is a thin

film of thickness d_{gr} on the order of nanometers. As seen in Figure 1, a three-dimensional free standing graphene monolayer configuration will yield the same results described by two-dimensional conductivity. Hence, the photon propagation of light inside the nonlinear monolayer can be expressed as the non-homogeneous vector Helmholtz's equation as follows [8]:

$$c^2 \epsilon_0 \left[\left(\frac{n_s}{c} \right)^2 \frac{\partial^2}{\partial t^2} - \nabla^2 \right] \mathbf{A}(\mathbf{r}, t) = \mathbf{j}_{NL}(\mathbf{r}, t), \quad (1)$$

where $\mathbf{A}(\mathbf{r}, t)$ is the magnetic potential vector, and n_s is the linear refractive index of graphene. To solve Eq. (1), we assume a solution of the form

$$\mathbf{A}(\mathbf{r}, t) = \frac{1}{2} \left\{ \hat{\mathbf{A}}(x) F(z, y) \exp[i(\beta z - \omega t)] + c.c. \right\}, \quad (2)$$

where $\hat{\mathbf{A}}(x)$ is an arbitrary integrable function that governs the confinement and polarization of the EM field along the x -direction, and $c.c.$ is the complex conjugate of the former term. Moreover, the EM field in the graphene plane is then governed by the complex function $F(z, y)$, and the propagation constant along the z -direction is given by β . Now, we insert Eq. (2) into Eq. (1), apply the slowly varying amplitude approximation, and project both sides of the resulting equation over the transpose conjugate $[\hat{\mathbf{A}}(x)]^{*T}$. The auxiliary function is taken to be $f(z, y) \equiv F(z, y) \exp(-i\phi z)$ (where $\phi \equiv (k_s^2 - \beta^2 + I_2/I_1)/2$, $k_s = n_s^2 \omega^2 / c^2$, $I_1 \equiv \int_{-\infty}^{\infty} |\hat{\mathbf{A}}(x)|^2 dx$ and $I_2 \equiv \int_{-\infty}^{\infty} dx [\hat{\mathbf{A}}(x)]^{*T} \partial^2 \hat{\mathbf{A}}(x) / \partial x^2$). As such, Eq. (1) can be solved in terms of the auxiliary function $f(z, y)$ as

$$2i\beta \frac{\partial f(z, y)}{\partial z} + \frac{\partial^2 f(z, y)}{\partial y^2} + g |f(z, y)|^2 f(z, y) = 0, \quad (3)$$

where $g \equiv \frac{3}{4} \omega^4 \chi_{gr}^{(3)} I_3 / I_1 c^2$, and $I_1 \equiv \int_{-d_{gr}/2}^{d_{gr}/2} |\hat{\mathbf{A}}(x)|^4 dx$. Eq. (3) corresponds to the nonlinear Schrödinger equation (NLSE), whose bright soliton solutions have the form [11, 12]

$$f(z, y) = \frac{1}{w} \sqrt{\frac{2}{g}} \operatorname{sech}\left(\frac{y}{w}\right) \exp\left(\frac{iz}{2\beta w^2}\right). \quad (4)$$

Here, w defines the soliton width and $\chi_{gr}^{(3)}$ is the Kerr-type third-order effective nonlinear susceptibility. Solving the auxiliary function this way permits a simple and effective way to solve Eq. (2), which calculates the electric field as $\mathbf{E}(\mathbf{r}, t) = -\partial \mathbf{A}(\mathbf{r}, t) / \partial t$. The propagation of light in a waveguide by which the refractive index contrasts between the core and the cladding is described physically by Eqs. (3) and (4). More importantly, Eq. (4) shows mathematically that optical solitons do indeed exist in graphene. From Eq. (3),

it can be seen that the interaction parameter g governs the graphene inhomogeneties. As such, a constant g will represent an ideal graphene monolayer configuration without defects. Similarly, a variable g will represent a more realistic graphene monolayer configuration that contains impurities or defects. It is of interest to study such graphene impurities to determine whether or not such deviations of the interaction parameter g induce optical scattering of the propagating soliton, especially in the case of large propagation distances. As pointed out in the previous section, for a constant g , Nesterov and co-workers [8] employed a finite element modeling to demonstrate that 2D graphene monolayers can support optical soliton propagation. In this study, we will investigate the optical soliton propagation in the case of a variable g . Because such deviation in g is rather difficult to simulate using finite element methods, we will utilize the explicit G-FDTD method to solve Eq. (3) with a variable g .

III. EXPLICIT G-FDTD SCHEME

To apply the explicit G-FDTD method in [9, 10] (the general idea of the G-FDTD dates back to Visscher [13]), we first assume that the auxiliary function $f(z, y)$ be a sufficiently smooth function which vanishes for sufficiently large $|y|$, and split the variable $f(z, y)$ into real and imaginary components,

$$f(z, y) = f_{\text{real}}(z, y) + i f_{\text{imag}}(z, y). \quad (5)$$

Inserting Eq. (5) into Eq. (3) and then separating the real and imaginary parts result in the following coupled set of equations:

$$\begin{aligned} \frac{\partial f_{\text{real}}(z, y)}{\partial z} &= -\frac{1}{2\beta} \left\{ \frac{\partial^2 f_{\text{imag}}(z, y)}{\partial y^2} + g [f_{\text{real}}^2(z, y) + f_{\text{imag}}^2(z, y)] f_{\text{imag}}(z, y) \right\} \\ &= -\frac{1}{2\beta} (A + g|f|^2) f_{\text{imag}}(z, y), \end{aligned} \quad (6)$$

where $A = \frac{\partial^2}{\partial y^2}$ and $|f|^2 = f_{\text{real}}^2(z, y) + f_{\text{imag}}^2(z, y)$.

We denote $f_{\text{real}}(k\Delta y, n\Delta z)$ as $f_{\text{real}}^n(k)$, and $f_{\text{imag}}(k\Delta y, n\Delta z)$ as $f_{\text{imag}}^n(k)$ for simplicity. Using a Taylor series expansion at $z = (n - 1/2)\Delta z$, we obtain

$$f_{\text{real}}^n(k) - f_{\text{real}}^{n-1}(k) = 2 \sum_{m=0}^M \left(\frac{\Delta z}{2}\right)^{2m+1} \frac{1}{(2m+1)!} \frac{\partial^{2m+1} f_{\text{real}}(y, z_{n-1/2})}{\partial z^{2m+1}} + O(\Delta z^{2M+3}) \quad (7a)$$

and

$$f_{\text{imag}}^n(k) - f_{\text{imag}}^{n-1}(k) = 2 \sum_{m=0}^M \left(\frac{\Delta z}{2}\right)^{2m+1} \frac{1}{(2m+1)!} \frac{\partial^{2m+1} f_{\text{imag}}(y, z_{n-1/2})}{\partial z^{2m+1}} + O(\Delta z^{2M+3}). \quad (7b)$$

We then evaluate those derivatives in Eq. (7a) by using Eqs. (6a) and (6b) repeatedly, where z in $f_{\text{real}}^2(z, y) + f_{\text{imag}}^2(z, y)$ is fixed at $(n - 1/2)\Delta z$:

$$\frac{\partial f_{\text{real}}(y, z_{n-1/2})}{\partial z} = -\frac{1}{2\beta} \left(A + g |f^{n-1/2}|^2 \right) f_{\text{imag}}(y, z_{n-\frac{1}{2}}), \quad (8a)$$

$$\begin{aligned} \frac{\partial^3 f_{\text{real}}(y, z_{n-1/2})}{\partial z^3} &= -\frac{1}{2\beta} \left(A + g |f^{n-1/2}|^2 \right) \frac{\partial^2 f_{\text{imag}}(y, z_{n-1/2})}{\partial z^2} \\ &= \frac{1}{2\beta} \left(A + g |f^{n-1/2}|^2 \right) \frac{1}{2\beta} \left(A + g |f^{n-1/2}|^2 \right) \frac{\partial f_{\text{real}}(y, z_{n-1/2})}{\partial z} \\ &= \left[\frac{1}{2\beta} (A + g |f^{n-1/2}|^2) \right]^3 f_{\text{imag}}(y, z_{n-\frac{1}{2}}), \end{aligned} \quad (8b)$$

$$\begin{aligned} \frac{\partial^5 f_{\text{real}}(y, z_{n-1/2})}{\partial z^5} &= \left[\frac{1}{2\beta} (A + g |f^{n-1/2}|^2) \right]^3 \frac{\partial^2 f_{\text{imag}}(y, z_{n-1/2})}{\partial z^2} \\ &= - \left[\frac{1}{2\beta} (A + g |f^{n-1/2}|^2) \right]^3 \left[\frac{1}{2\beta} (A + g |f^{n-1/2}|^2) \right] \frac{\partial f_{\text{real}}(y, z_{n-1/2})}{\partial z} \\ &= - \left[\frac{1}{2\beta} (A + g |f^{n-1/2}|^2) \right]^5 f_{\text{imag}}(y, z_{n-\frac{1}{2}}), \end{aligned} \quad (8c)$$

and so on, where $|f^{n-1/2}|^2 = f_{\text{real}}^2(k\Delta y, z_{n-1/2}) + f_{\text{imag}}^2(k\Delta y, z_{n-1/2})$. Substituting Eq. (8) and other similar equations into Eq. (7a) gives

$$\begin{aligned} f_{\text{real}}^n(k) - f_{\text{real}}^{n-1}(k) &= 2 \sum_{m=0}^M \left(\frac{\Delta z}{2} \right)^{2m+1} \frac{(-1)^m}{(2m+1)!} \left[-\frac{1}{2\beta} (A + g |f^{n-1/2}|^2) \right]^{2m+1} f_{\text{imag}}(y, z_{n-\frac{1}{2}}) \\ &\quad + O(\Delta z^{2M+3}). \end{aligned} \quad (9)$$

Similarly, using Eqs. (6a) and (6b) repeatedly to evaluate those derivatives in Eq. (7b), we obtain

$$\frac{\partial f_{\text{imag}}(y, z_{n-1/2})}{\partial z} = \frac{1}{2\beta} \left(A + g |f^{n-1/2}|^2 \right) f_{\text{real}}(y, z_{n-\frac{1}{2}}), \quad (10a)$$

$$\begin{aligned} \frac{\partial^3 f_{\text{imag}}(y, z_{n-1/2})}{\partial z^3} &= \frac{1}{2\beta} \left(A + g |f^{n-1/2}|^2 \right) \frac{\partial^2 f_{\text{real}}(y, z_{n-1/2})}{\partial z^2} \\ &= -\frac{1}{2\beta} \left(A + g |f^{n-1/2}|^2 \right) \frac{1}{2\beta} \left(A + g |f^{n-1/2}|^2 \right) \frac{\partial f_{\text{imag}}(y, z_{n-1/2})}{\partial z} \\ &= - \left[\frac{1}{2\beta} (A + g |f^{n-1/2}|^2) \right]^3 f_{\text{real}}(y, z_{n-\frac{1}{2}}), \end{aligned} \quad (10b)$$

$$\begin{aligned}
\frac{\partial^5 f_{\text{imag}}(y, z_{n-1/2})}{\partial z^5} &= - \left[\frac{1}{2\beta} (A + g |f^{n-1/2}|^2) \right]^3 \frac{\partial^2 f_{\text{real}}(y, z_{n-1/2})}{\partial z^2} \\
&= \left[\frac{1}{2\beta} (A + g |f^{n-1/2}|^2) \right]^3 \left[\frac{1}{2\beta} (A + g |f^{n-1/2}|^2) \right] \frac{\partial f_{\text{imag}}(y, z_{n-1/2})}{\partial z} \\
&= \left[\frac{1}{2\beta} (A + g |f^{n-1/2}|^2) \right]^5 f_{\text{real}}(y, z_{n-\frac{1}{2}}), \tag{10c}
\end{aligned}$$

and so on. Substituting Eq. (10) and other similar equations into Eq. (7b) gives

$$\begin{aligned}
f_{\text{imag}}^n(k) - f_{\text{imag}}^{n-1}(k) &= 2 \sum_{m=0}^M \left(\frac{\Delta z}{2} \right)^{2m+1} \frac{(-1)^{m+1}}{(2m+1)!} \left[-\frac{1}{2\beta} (A + g |f^{n-1/2}|^2) \right]^{2m+1} f_{\text{real}}(y, z_{n-\frac{1}{2}}) \\
&\quad + O(\Delta z^{2M+3}). \tag{11}
\end{aligned}$$

Noting that the term $|f^{n-1/2}|^2$ in Eqs. (9) and (11) needs to be evaluated, we use a similar argument and obtain

$$\begin{aligned}
f_{\text{real}}^{n+1/2}(k) - f_{\text{real}}^{n-1/2}(k) &= 2 \sum_{m=0}^M \left(\frac{\Delta z}{2} \right)^{2m+1} \frac{(-1)^m}{(2m+1)!} \left[-\frac{1}{2\beta} (A + g |f^n|^2) \right]^{2m+1} f_{\text{imag}}(y, z_n) \\
&\quad + O(\Delta z^{2M+3}), \tag{12a}
\end{aligned}$$

$$\begin{aligned}
f_{\text{imag}}^{n+1/2}(k) - f_{\text{imag}}^{n-1/2}(k) &= 2 \sum_{m=0}^M \left(\frac{\Delta z}{2} \right)^{2m+1} \frac{(-1)^{m+1}}{(2m+1)!} \left[-\frac{1}{2\beta} (A + g |f^n|^2) \right]^{2m+1} f_{\text{real}}(y, z_n) \\
&\quad + O(\Delta z^{2M+3}), \tag{12b}
\end{aligned}$$

where $|f^n|^2 = f_{\text{real}}^2(k\Delta y, z_n) + f_{\text{imag}}^2(k\Delta y, z_n)$. Next, we couple Eqs. (9), (11) and (12) together, drop out the truncation error $O(\Delta z^{2M+3})$, and replace $\frac{\partial^2}{\partial x^2}$ by a fourth-order accurate central difference operator, $\frac{1}{\Delta y^2} D_y^2 u(k) = \frac{1}{12\Delta y^2} [-u(k+2) + 16u(k+1) - 30u(k) + 16u(k-1) - u(k-2)]$. This results in our explicit G-FDTD scheme for solving Eq. (3) as follows:

$$f_{\text{real}}^n(k) - f_{\text{real}}^{n-1}(k) = 2 \sum_{m=0}^M \frac{(-1)^m}{(2m+1)!} \left[-\frac{1}{2\beta} \left(\frac{\sigma}{2} D_y^2 + \frac{\lambda\Delta z}{2} |f^{n-1/2}|^2 \right) \right]^{2m+1} f_{\text{imag}}^{n-1/2}(k), \tag{13a}$$

$$f_{\text{imag}}^n(k) - f_{\text{imag}}^{n-1}(k) = 2 \sum_{m=0}^M \frac{(-1)^{m+1}}{(2m+1)!} \left[-\frac{1}{2\beta} \left(\frac{\sigma}{2} D_y^2 + \frac{\lambda\Delta z}{2} |f^{n-1/2}|^2 \right) \right]^{2m+1} f_{\text{real}}^{n-1/2}(k); \tag{13b}$$

$$f_{\text{real}}^{n+1/2}(k) - f_{\text{real}}^{n-1/2}(k) = 2 \sum_{m=0}^M \frac{(-1)^m}{(2m+1)!} \left[-\frac{1}{2\beta} \left(\frac{\sigma}{2} D_y^2 + \frac{\lambda\Delta z}{2} |f^n|^2 \right) \right]^{2m+1} f_{\text{imag}}^n(k), \tag{13c}$$

$$f_{\text{imag}}^{n+1/2}(k) - f_{\text{imag}}^{n-1/2}(k) = 2 \sum_{m=0}^M \frac{(-1)^{m+1}}{(2m+1)!} \left[-\frac{1}{2\beta} \left(\frac{\sigma}{2} D_y^2 + \frac{\lambda\Delta z}{2} |f^n|^2 \right) \right]^{2m+1} f_{\text{real}}^n(k); \tag{13d}$$

where $\sigma = \Delta z / \Delta y^2$. Thus, once $f_{\text{imag}}^{n-1}(k)$, $f_{\text{real}}^{n-1}(k)$, $f_{\text{imag}}^{n-1/2}(k)$ and $f_{\text{real}}^{n-1/2}(k)$ are given, one may explicitly calculate $f_{\text{real}}^n(k)$ and $f_{\text{imag}}^n(k)$ using Eqs. (13a) and (13b), and then obtain $f_{\text{real}}^{n+1/2}(k)$ and $f_{\text{imag}}^{n+1/2}(k)$ using Eqs. (13c) and (13d). It is an explicit iteration, and therefore the computation is simple and fast. The stability of the explicit G-FDTD scheme for solving the NLSE and the discrete conservation law that the scheme satisfies can be seen in [9]. It can be seen that the truncation error between the above scheme and Eqs. (9), (11) and (12) is $O(\Delta y^4 + \Delta z^{2M+3})$. However, the truncation error between the above scheme and the original NLSE, Eq. (3), may be different because the z in the term $|f(z, y)|^2$ is fixed in the small z interval either (z_{n-1}, z_n) or $(z_{n-1/2}, z_{n+1/2})$ in the above derivation. Furthermore, it should be pointed out that the partial derivative $\frac{\partial^2}{\partial y^2}$ can alternatively be approximated using a spectral, or other higher-order method. In this study, we confine our attention to the finite-difference method with a fourth-order central difference approximation.

IV. OPTICAL SOLITON SIMULATION

We first calculated the electric field $|\mathbf{E}(\mathbf{r}, t)|$ along a free-standing non-linear layer, where $g = 5$, $w = 2$, $\beta = -0.5$, and $\phi = \omega = 1$ in Eqs. (1) - (4), where the parameters represent a free-standing graphene monolayer configuration in the absence of defects. This can be done by injecting optical solitons at one edge of the monolayer. The initial condition was chosen to be a bright soliton based on the analytical solution

$$f(z, y) = \frac{1}{w} \sqrt{\frac{2}{g}} \text{sech}\left(\frac{y}{w}\right) \exp\left(\frac{iz}{2\beta w^2}\right), \quad (14)$$

and $\hat{\mathbf{A}}(x) = \frac{1}{1+x^2}$ in Eq. (2). The purpose of this calculation was for comparison with the results of Nesterov et al. [8]. In our computation, the domain was taken to be $-10 \leq x, y \leq 10$, $0 \leq z \leq 1$. The solution was defined to be analytical outside the computational domain for simplicity. We chose $M = 1$ in our scheme in Eq. (13), and the number of grid points in x and y to be 200 with $\Delta z = 0.01$. Our G-FDTD methods are used to evolve Eq. (14) in the z -direction simulating the propagation of the soliton into the material after being injected at $z = 0$ (see Fig. 1). In all of our simulations, after sufficient propagation in the z direction $f(z, y)$ reaches steady-state. This solution was then substituted into Eq. (2) to obtain the vector potential $\mathbf{A}(\mathbf{r}, t)$. The electric field within the monolayer was then calculated according to $\mathbf{E}(\mathbf{r}, t) = -\partial \mathbf{A}(\mathbf{r}, t) / \partial t$, giving our results as shown in Fig. 2. It can

be seen from Fig. 2 that our G-FDTD method has produced the similar result as obtained by Nesterov et al. (see Fig. 2 in [8]).

In order to study the effect of point defects in a free-standing nonlinear layer on bright optical soliton behavior, g in Eq. (3) was varied such that at $y = 0$, $g = 0.5$, and everywhere else $g = 0.05$. As before, the optical field was injected with the profile as given in Eq. (14) at $z = 0$ and was evolved in z according to Eq. (3) by the G-FDTD method. We found that beyond $z > 1$, the auxiliary function $f(z, y)$ remains the same for all z , and thus steady-state has been reached. The electric field $|\mathbf{E}(\mathbf{r}, t)|$ is then calculated for the times $0 \leq t \leq 10$ in increments of $t = 2$ as seen in Fig. 3. It can be seen that the general soliton shape is preserved even in the presence of the defect, with dips present corresponding to its location. The oscillation in time is seen for the same reasons as Fig. 2, where the electric field oscillates due to the energy exchange with the magnetic field. We observed no significant scattering of the optical soliton due to the defect, with its overall shape being unchanged during oscillation of the electric field over time. This can be interpreted as an analogous effect to superfluidity [14], where a fluid can flow with reduced scattering in the presence of defects. In a standard fluid the presence of defects creates scattering which eventually impedes the propagation of the fluid by reflections which randomize the momentum of the incident wave. In a superfluid below the critical velocity, such backscattering events become energetically suppressed leading to resistanceless flow. Similar effects in polaritonic media have been observed [15].

Furthermore, we examined the robustness of the soliton propagation in the presence of multiple point defects placed in a free-standing monolayer configuration. This was performed numerically in the same way by varying g in Eq. (3) such that at the y -location of the defect, $g = 0.5$, and everywhere else $g = 0.05$. As seen in the single defect case, the bright soliton preserves its shape despite presence of the graphene defect(s). The electric field $|\mathbf{E}(\mathbf{r}, t)|$ at $t = 0$ as seen in Fig. 4 demonstrates the presence of zero to five point defects. The numerical solutions show very stable configurations despite starting from the initial conditions Eq. (14). The steady state configuration is reached after numerical evolution to $z = 1$ and remains unchanged beyond this distance. Again the the solitons show oscillations in the time domain, hence we show results for $t = 0$. The location of the defects create local dips in the magnitude of the electric field but otherwise show the same soliton profile as the defect-free solution. These results show that the graphene monolayer serves as a

highly robust material that can propagate optical solitons even in the presence of defects. The results also show that the explicit G-FDTD can handle strong variations in g along y without diverging. Similar finite element methods tend to give diverging results for spatially varying g , particularly for large variations such as considered here.

V. CONCLUSION

We have performed a numerical study of bright optical solitons, and shown how various material configurations can affect behavior of the electric field along a free-standing nonlinear layer, including defects. It was found that optical solitons can travel in such monolayers taking advantage of the natural nonlinearity that is present in these materials. Our simulations indicate that even in the presence of defects, the solitons can travel large distances with the overall shape of the solitons being unchanged beyond local variations at the defect position. This can be interpreted to be caused by the beneficial effects of the nonlinearity. The nonlinear interaction gives a suppressed scattering due to an effect analogous to superfluidity. This allows the optical soliton to propagate even in the presence of the defects, which would otherwise destroy the soliton due to multiple backscattering events. These results show that beyond the self-guiding nature of the nonlinear monolayer, such materials are beneficial as they are rather robust even in the presence of graphene imperfections.

The numerical simulations were performed using the recently developed G-FDTD method for solving an analogue of the non-homogeneous vector Helmholtz's equation. The large spatial variations in g are efficiently simulative thanks to the improved stability of the G-FDTD algorithm. Comparable simulations using standard finite element methods would require much smaller evolution steps Δz in order to obtain convergent results. Results show that the G-FDTD scheme provides an accessible technique for studying dynamic solutions of the magnetic vector potential $\mathbf{A}(\mathbf{r}, t)$ and electric field $\mathbf{E}(\mathbf{r}, t)$ corresponding to a free-standing graphene monolayer configuration in $3 + 1$ dimensions. This makes the method appropriate suitable for studying more complex geometrical configurations such as optical networks based on the monolayers. We leave this and other extensions of the study as future work.

Acknowledgments

This research is supported by grant #FA8650-05-D-1912 from the United States Air Force Office of Scientific Research and a grant from the NASA EPSCoR & LaSPACE, Louisiana. The second author is supported by the Okawa Foundation.

- [1] Novoselov et al., *Science* 306 (2004) 666.
- [2] F. Bonaccorso, Z. Sun, T. Hasan, and A. C. Ferrari, *Nature Photon.* 4 (2010) 611.
- [3] M. Liu, X. Yin, E. Ulin-Avila, B. Geng, T. Zentgraf, L. Ju, F. Wang, and X. Zhang, *Nature* 474 (2011) 64.
- [4] S. A. Mikhailov, *Europhys. Lett.* 79 (2007) 27002.
- [5] K. L. Ishikawa, *Phys. Rev. B* 82 (2010) 201402.
- [6] Y. V. Kartashov, B. A. Malomed, and L. Torner, *Rev. Mod. Phys.* 83 (2011) 247.
- [7] Y. Liu, G. Bartal, D. Genov, and X. Zhang, *Phys. Rev. Lett.* 99 (2007) 153901.
- [8] M. L. Nesterov, J. Bravo-Abad, A. Y. Nikitin, F. J. Garcia-Vidal, and L. Martin-Moreno, *Laser Photonics Rev.* 7 (2012) L7.
- [9] F. I. Moxley III, D.T. Chuss, and W. Dai, *Comput. Phys. Commun.* 184 (2013) 1834.
- [10] F. I. Moxley III, T. Byrnes, F. Fujiwara, and W. Dai, *Comput. Phys. Commun.* 183 (2012) 2434.
- [11] Y. Kivshar and G. Agrawal, *Optical Solitons* (Academic Press, New York, 2003).
- [12] R. W. Boyd, *Nonlinear Optics* (Academic Press, New York, 1992).
- [13] P. B. Visscher, *Comput. Phys.* 5 (1991) 596.
- [14] L. Pitaevskii and S. Stringari, *Bose-Einstein Condensation* (Oxford University Press, 2003).
- [15] M. Wouters and I. Carusotto, *Phys. Rev. Lett.* 105 (2010) 020602.

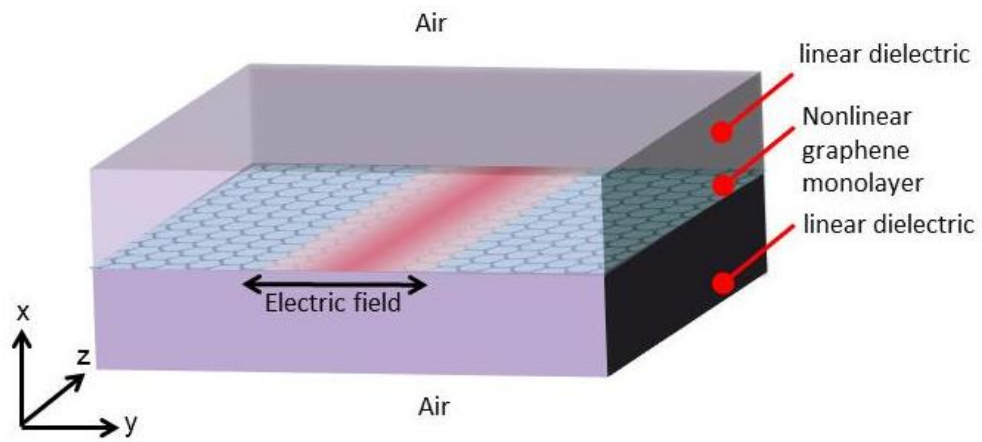


FIG. 1. Geometry and optical soliton formation as the intensity of a propagating beam is evaluated at the graphene monolayer within a dielectric waveguide.

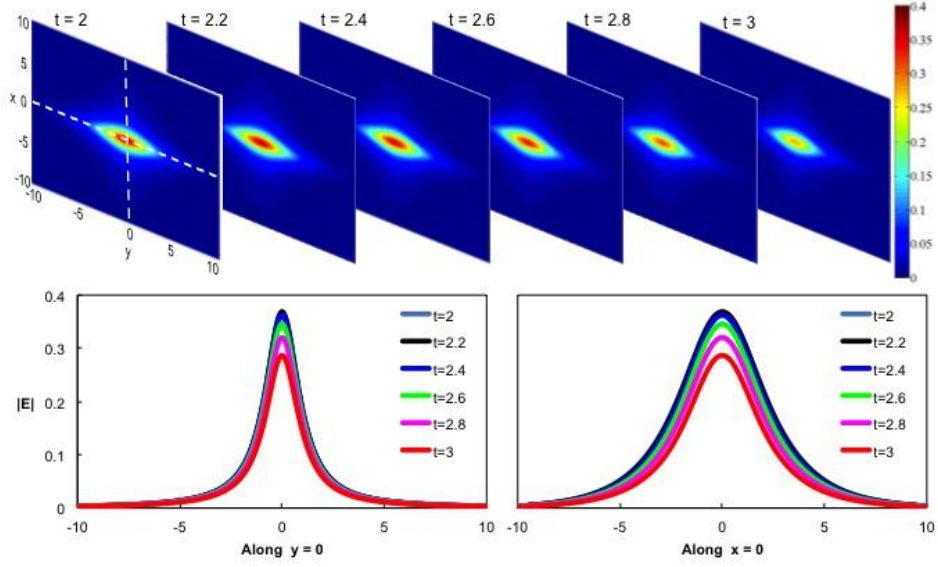


FIG. 2. Simulation of the electric field distribution $|\mathbf{E}(\mathbf{r},t)|$ in a graphene monolayer with a bright optical soliton ($g = 5.0$), where the G-FDTD scheme was employed with $\Delta z = 0.01$, $\Delta x = \Delta y = 0.1$, $w = 2.0$, $\beta = -0.5$, $z=1$, and $\phi = \omega = 1.0$ at various times (t).

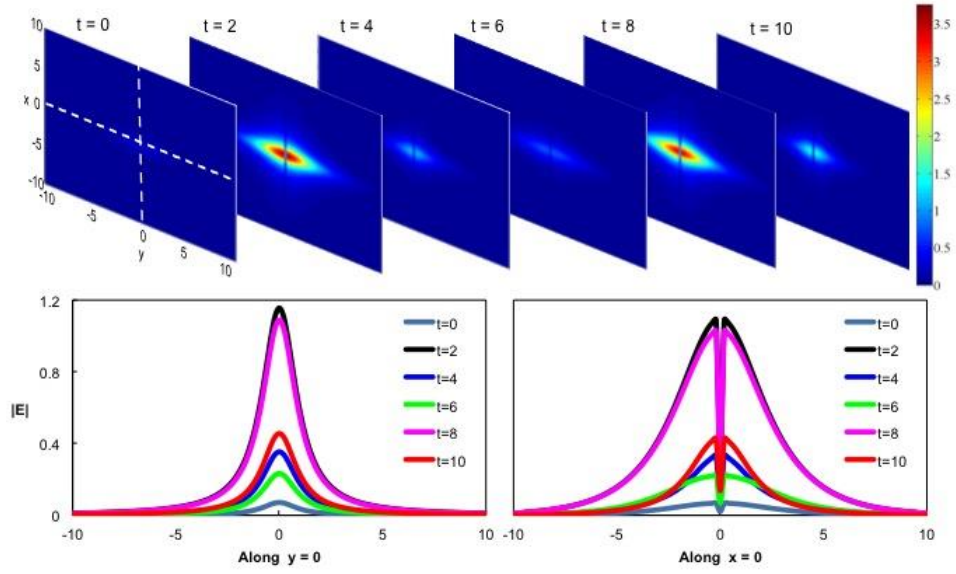


FIG. 3. Simulation of the electric field distribution $|\mathbf{E}(\mathbf{r},t)|$ in a graphene monolayer with a bright optical soliton ($g = 0.05$) and defect ($g = 0.5$), where the G-FDTD scheme was employed with $\Delta z = 0.01$, $\Delta x = \Delta y = 0.1$, $w = 2.0$, $\beta = -0.5$, $z=1$, and $\phi = \omega = 1.0$ at various times (t).

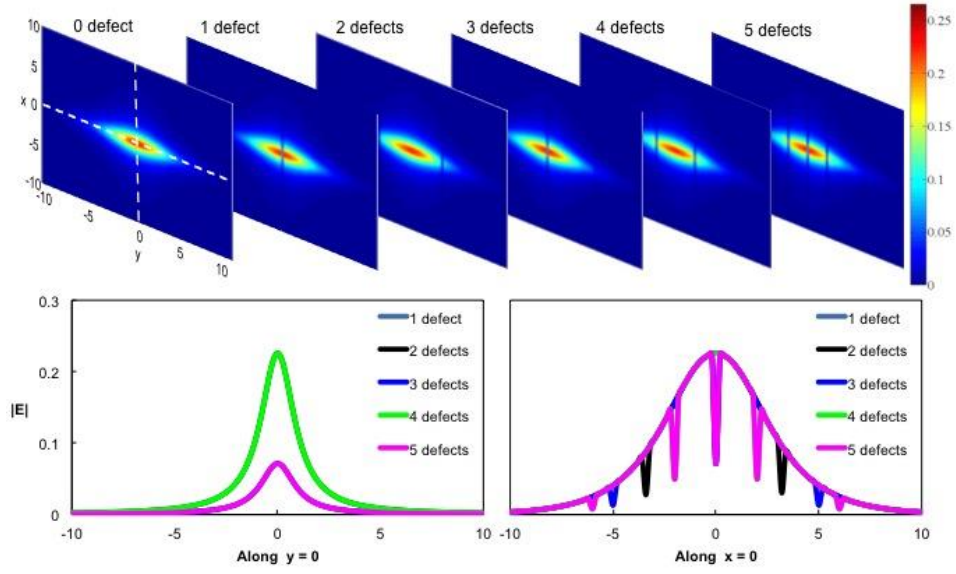


FIG. 4. Simulation of the electric field distribution $|\mathbf{E}(\mathbf{r}, t)|$ in a graphene monolayer with a bright optical soliton ($g = 0.05$) and defect(s) ($g = 0.5$), where the G-FDTD scheme was employed with $\Delta z = 0.01$, $\Delta x = \Delta y = 0.1$, $w = 2.0$, $\beta = -0.5$, $z=1$, $t=0$ and $\phi = \omega = 1.0$ with a various numbers of defects.